

## Recovery of Submicron-Sized Silicon-Rich Powder from Silicon Sawing Waste for Electrocatalyst of Methanol Electrooxidation

Tzu-Hsuan Tsai<sup>1</sup> and Yung-Fu Wu<sup>2,\*</sup>

<sup>1</sup> Department of Materials and Mineral Resources Engineering, National Taipei University of Technology, Taipei 10608, Taiwan

<sup>2</sup> Department of Chemical Engineering, Ming Chi University of Technology, New Taipei City 24301, Taiwan

\*E-mail: [gausswu@mail.mcut.edu.tw](mailto:gausswu@mail.mcut.edu.tw)

*Received:* 14 June 2017 / *Accepted:* 25 July 2017 / *Published:* 5 June 2018

---

This study proposed a feasible process for recovering Si-rich powder at room temperature for electrocatalyst applications. The proposed process was successively performed through ultrasonic treatment for particle dispersion, magnetic separation for metal removal, and centrifugation for size classification. The experimental results indicated that the recovered Si-rich powder contained 85 wt.% Si and 346 ppm Fe. Subsequently, the recovered powder was directly mixed with carbon to prepare an electrocatalyst for methanol electrooxidation. Our study indicated that the electrocatalytic applications of fine Si powder may be a suitable incentive to recycle Si from sawing waste.

---

**Keywords:** Recovery, Silicon, Iron, Sawing Waste, Magnetic Separation, Centrifugation, Electrocatalyst

### 1. INTRODUCTION

Si wafers are formed by cutting an ingot through wire saws and slurries containing glycol and Si carbide abrasives. However, more than 40% of Si in each ingot changes into sawing kerf [1]. Therefore, typical sawing waste comprises glycol, kerf Si, SiC, and metal fragments from the wire saw. Because of the growing need for wafers, substantial sawing waste is produced. This waste not only strongly affects the environment but also results in a high disposal cost. To reduce this sawing waste, researchers should develop approaches for recycling kerf Si, abrasives, and glycol liquids [2].

A recent study proposed that recovered Si can be used to fabricate solar cells; however, removing SiC from the waste is the main challenge [3]. Ciftja et al. used foam filtration to remove SiC and Si<sub>3</sub>N<sub>4</sub> from the top-cut Si scraps of solar cells [4, 5]. Wang et al. developed a purification process

including chemical treatment, heavy-fluid high-gravity centrifugation, high-temperature treatment, and directional solidification [6, 7]. Li et al. proposed procedures involving sedimentation, acid leaching, filtration, and high-temperature melting for fabricating high-purity Si from cutting slurry [8]. Lin et al. [9] and Xiao and Yang [10] employed a heavy liquid to recover Si from sawing waste. Huang et al. applied froth flotation to separate Si from sawing waste [11]. Lin and Tai [12] and Hsu et al. [13] used the hydrophobicity difference between Si and SiC to recover Si from kerf-loss slurry waste. Wang et al. [14] and Li et al. [15] proposed Al–Si and Cu–Si alloying processes to remove SiC from sawing waste. Tomono et al. used a bromination process to extract pure Si from sawing waste [16]. Liu et al. separated Si by tuning the surface potential of particles [17]. Furthermore, several researchers have attempted to separate metal fragments from Si sawing waste. Nishijima et al. applied a superconducting magnetic method to acquire SiC from sawing waste [18]. Hariharan and Ravi used a filter bed to remove metal halides generated during Si recovery [19]. Hoffmann used floatation to separate metals from Si [20]. Wang et al. [6,7] and Lin et al. [9] employed concentrated nitric acid to remove Cu and Fe fragments from sawing waste. Li et al. [8] used 15 wt.% HCl to remove Fe from sawing waste.

In our previous studies, we presented methods that were based on acid treatment and electrokinetic separation for removing Fe from sawing waste [21, 22]. Furthermore, we proposed a gravitational settling system under an electric field and a magnetic field for recovering Si from sawing waste. In that system, the removal fraction of Fe was more than 99.9%, and the Si content in the recovered powder reached 88 wt.% [23]. However, considerable time and electricity consumption were required because of the slow settling of submicron-sized particles. Moreover, the fine particles of the recovered Si were readily oxidized on their surface. If these particles would be used to produce solar cells, additional purification steps would be required, and the product yield may be insufficient. Nevertheless, submicron-sized Si and SiO<sub>2</sub> powders have been widely used to prepare electrocatalysts, such as those used for oxygen reduction [24], methanol electrooxidation [25], and ethanol electrooxidation [26]. Therefore, this study proposed a feasible process for obtaining Si-rich powder from Si sawing waste. The proposed process was performed at room temperature and did not require an electric field or extra chemicals. After obtaining Si-rich powder (res-Si), we added the powder to a carbon support for fabricating a Pt electrocatalyst (Pt/C/res-Si), and we then compared the performance of Pt/C/res-Si with that of Pt/C or Pt/C/pure Si for methanol electrooxidation. Through our study, we attempted to demonstrate the electrocatalyst applications of the recycled Si from the sawing waste and thus increase the motivation to recycle Si from sawing waste.

## 2. MATERIALS AND METHODS

### 2.1. Properties and composition of waste

Sino-American Silicon Products, Inc. (Chu-Nan, Taiwan) supplied the sawing waste for this study. Most of the large SiC particles (approximately 10 μm) were removed in the factory. Samples were washed using acetone, centrifuged at 10000 rpm for 30 min to form a wet cake, and then dried in

an oven at 120°C to form solid powder. The liquid content in the sample was determined based on mass loss. Subsequently, to dissolve the metal, the powder samples were mixed with 5.2 M HNO<sub>3(aq)</sub> in an oscillating shaker. After filtration, a filtrate with low levels of metals was obtained. The metal content in the filtrate was analyzed using an inductively coupled plasma-optical emission spectrometer (ICP-OES, Perkin Elmer 3100XL). Furthermore, the powder was mixed with 0.5 M NaOH<sub>(aq)</sub> to dissolve Si, and the Si content in the filtrate was also analyzed using the ICP-OES.

The microstructural features and composition of the powder were examined using a scanning electron microscope (SEM) (model: S-4700, Hitachi) and energy dispersive X-ray spectroscopy (EDS) (model: 7200-H, Horiba). Additionally, the particle size distributions (PSDs) of the waste were measured using a static light scattering instrument (model: LA300, Horiba). The viscosity of the waste was measured using a viscometer (model: LVDV-I Prime, Brookfield).

## 2.2. Magnetic separation

A magnetic separator (model: WHIMS-3X4L, Carpc Inc.) was used to apply 0.1–0.44 T magnetic fields by controlling the voltages and currents of the magnetic coil. Stainless steel wool used as a magnetic filter was placed in a matrix canister to induce magnetic fields. Figure 1 illustrates the setup. When the waste passed through the magnetic filter with the induced magnetic field, four main forces, as shown in the insert of Fig. 1, were exerted on a magnetic particle, namely gravitational force ( $F_g$ ), buoyant force ( $F_B$ ), drag force ( $F_D$ ), and magnetic force ( $F_M$ ). Assume that these particles are spherical and obey Stokes' law when the Reynolds number is lower than 0.1. Subsequently,  $F_g$ ,  $F_B$ , and  $F_D$  can be expressed as follows:

$$F_g = \frac{1}{6} \pi d_p^3 \rho_p g \quad (1)$$

$$F_B = \frac{1}{6} \pi d_p^3 \rho_l g \quad (2)$$

$$F_D = 3\pi\mu_l d_p (\mathbf{v}_f - \mathbf{v}_p) \quad (3)$$

where  $d_p$  is the particle diameter,  $\rho_p$  is the particle density,  $\rho_l$  is the liquid density,  $g$  is the gravitational acceleration,  $\mu_l$  is the liquid viscosity,  $\mathbf{v}_f$  is the fluid velocity, and  $\mathbf{v}_p$  is the particle velocity.

The magnetic force acting on a spherical magnetic particle inside a magnetic field can be expressed as follows [27, 28]:

$$F_M = \frac{1}{6} \pi d_p^3 \frac{\Delta\chi}{\mu_0} (B \cdot \nabla) B \quad (4)$$

where  $\Delta\chi$  is the difference in magnetic susceptibilities between the particle and the surrounding medium,  $\mu_0$  is the vacuum permeability ( $4\pi \times 10^{-7}$  T·m/A), and  $B$  is the applied magnetic field. If the magnetic force on a particle is higher than the other forces, the particle can be separated from the flowing waste by using the magnetic separator. In this study, the effects of fluid viscosity, the applied magnetic field, and the cycle number of passing through the magnetic filter on metal removal were

investigated. To adjust fluid viscosity, deionized water was added and mixed with the Si sawing waste by stirring for 5 min.

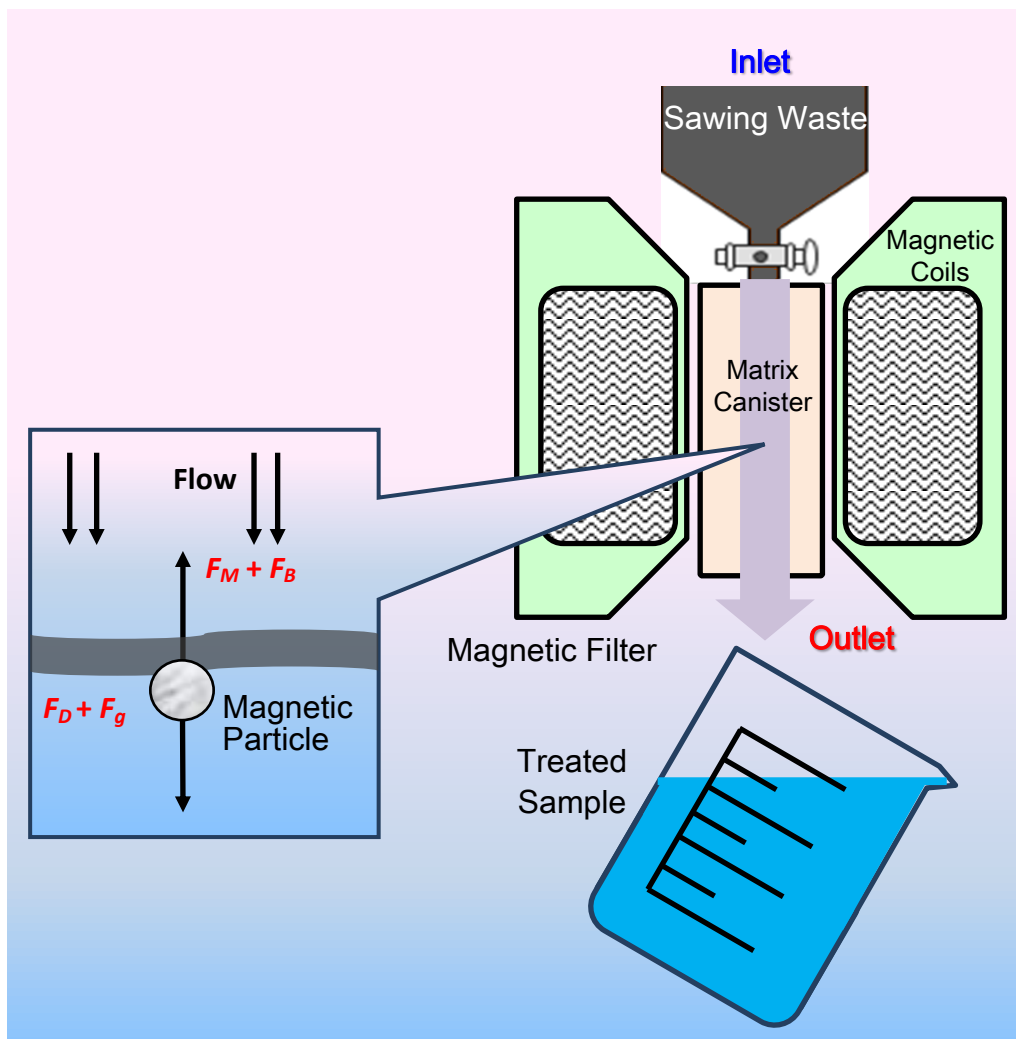


**Figure 1.** Magnetic separation setup and a schematic diagram of the main forces exerted on a magnetic particle.

The composition of the waste collected at the outlet of the magnetic separator was analyzed. The metal removal fraction  $R_M$  was calculated as follows:

$$R_M = 1 - \frac{c}{c_0} \tag{5}$$

where  $c_0$  is the initial metal concentration in the solid powder, and  $c$  is the residual metal concentration after separation.

### 2.3. Centrifugal separation

After magnetic separation, the treated waste was added to a centrifuge tube. Subsequently, a Hermle Z323K centrifuge with a 25° fixed angle rotor was applied to recover submicron-sized Si from the waste because the density and size of the Si particles were smaller than those of the SiC particles. Assume that the settling particles obey Stokes law and move along the axial direction of the centrifuge tube. The particle settling velocity ( $v_s$ ) in a centrifugal field can be estimated using the following equation [29]:

$$v_s = \frac{dx}{dt} = \frac{(\rho_p - \rho_l) \cdot d_p^2 \cdot r \omega^2}{18\mu_l} (1 - \varphi)^{4.65} \quad (6)$$

where  $d_p$ ,  $\rho_p$ ,  $\rho_l$ , and  $\mu_l$  are the particle diameter, particle density, liquid density, and liquid viscosity, respectively;  $\omega$  is the rotational speed of the centrifuge. In addition,  $(1 - \varphi)^{4.65}$  is the hindered settling function developed by Richardson and Zaki [30], and  $\varphi$  is the solid volume fraction in suspension. The radius  $r$  is equal to  $x \sin \theta$ ;  $L$  is the length occupied by the waste sample in the centrifuge tube, and  $T$  is the time required for a particle to travel through the tube from the top ( $x = x_0$ ) to the bottom ( $x = x_0 + L$ ). After integrating from  $x = x_0$  at  $t = 0$  to  $x = x_0 + L$  at  $t = T$ ,  $T$  can be expressed as follows:

$$T = \frac{18\mu_l}{(\rho_p - \rho_l) \cdot d_p^2 \cdot \omega^2 \sin \theta} (1 - \varphi)^{-4.65} \ln \left[ \frac{x_0 + L}{x_0} \right] \quad (7)$$

According to Eq. (7), SiC particles in the waste require a shorter time to travel through the tube than do Si particles. Therefore, the optimal centrifugation time and speed for obtaining submicron-sized Si (res-Si) in the upper liquid in the centrifuge tube were calculated. After centrifugation, the compositions of the upper liquid in the centrifuge tube were verified using the static light scattering instrument (model: LA300, Horiba).

### 2.4. Preparation and analysis of electrode catalyst

The res-Si was mixed with commercial carbon Vulcan XC-72 (C) at a mass ratio of C:Si = 9:1. Subsequently, 80 mg of the Si/C mixture was added to 50 mL of ethylene glycol with 2 mM of  $K_2PtCl_6$ . The solution was ultrasonically treated for 15 min. Subsequently, the pH of the mixture was adjusted to 10–11 by adding 0.5 M  $NaOH_{(aq)}$ , followed by refluxing the mixture at 120°C for 2–3 h to ensure complete reduction from  $PtCl_6^{2-}$  to Pt. After the reactions, the suspension liquid was filtered to obtain a filtrated cake. The cake was then washed with ethanol and deionized water, followed by drying at 120°C for 2 h to obtain a catalyst denoted as Pt/C/res-Si. For comparison, the same procedures were used to prepare Pt catalysts on commercial carbon Vulcan XC-72, denoted as Pt/C, and Pt on the mixture of carbon and pure Si powder (254 nm in diameter), denoted as Pt/C/Si. Ink was produced by mixing 2 mg of the prepared catalyst with a solution containing 1 mL of deionized water, 1 mL of ethanol, and 0.1 mL of 5 wt.% perfluorosulfonic acid. Subsequently, 5  $\mu$ L of the prepared ink was dropped on a glass carbon electrode (6 mm in diameter), followed by drying at room temperature.

The electrocatalytic reaction of methanol was then investigated through linear sweep voltammetry. A three-electrode system was used for the potential sweep. In the system, the glass carbon electrode covered with the proposed catalyst was employed as the working electrode, Pt wire as the counter electrode, and Ag/AgCl electrode as the reference electrode. Hence, the voltamogram was reported with respect to the potential of the Ag/AgCl electrode. The electrolyte composed of 0.5 M H<sub>2</sub>SO<sub>4</sub> and 1.0 M CH<sub>3</sub>OH was used to investigate methanol electrooxidation in a direct-methanol fuel cell. Before each cycle of electrocatalysis measurement, argon gas was injected through the electrolyte for 15 min. The potential sweep from 0.2 to 1.0 V versus the Ag/AgCl electrode at various scan rates was then controlled using an Autolab potentiostat (model: PGSTAT302N). The voltammograms of Pt/C, Pt/C/Si, and Pt/C/res-Si were obtained and analyzed, respectively.

### 3. RESULTS AND DISCUSSION

Prior to treatment, the sawing waste had a black and opaque appearance. The density and viscosity measured at 25°C were 1.09 g/cm<sup>3</sup> and 76 mPa·s, respectively. Figure 2 illustrates the PSD of the Si sawing waste, indicating that the main particle sizes were approximately 0.15 and 6.6 μm. Composition analysis indicated that the solid content in the waste was approximately 25.3 wt.%, and that the solid components of the waste were 39.1 wt.% Si, 58.5 wt.% SiC, and 2.37 wt.% metal (Fe = 20340 ppm, Cu = 2433 ppm, Zn = 899 ppm). These metal components were generated from broken steel wires during sawing, and the metal fragments may subsequently adhere to Si and SiC particles in the waste.

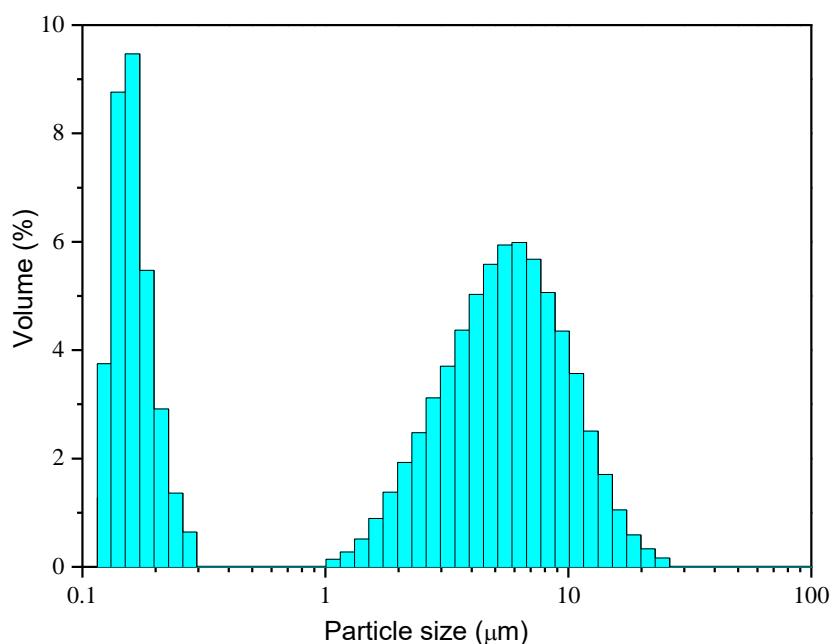


**Figure 2.** Particle size distribution of the obtained Si sawing waste.

The waste was introduced into the magnetic separator at a flow rate of 0.01 m/s. The result of magnetic separation is shown in Fig. 3, indicating that the Fe removal fraction increased when the applied magnetic field increased from 0.1 to 0.44 T. At 0.44 T, 48% of the Fe in the waste could be removed. Because Fe is ferromagnetic, the fragments containing Fe can be magnetized and attracted to the magnetic filter. If the physical properties of Fe fragments are substituted into Eqs. (1)–(3),  $F_g$ ,  $F_B$ , and  $F_D$  can be expressed with particle size,  $d_p$ , in SI units as follows:

$$F_g = (4.03 \times 10^4) \cdot d_p^3 \tag{8}$$

$$F_B = (5.59 \times 10^3) \cdot d_p^3 \tag{9}$$

$$F_D = (7.16 \times 10^{-3}) \cdot d_p \tag{10}$$

Because the saturated magnetization of the magnetic filter was 0.185 T, the approximate magnetic field gradient could be estimated by dividing the saturated magnetization by the wire diameter of the magnetic filter.

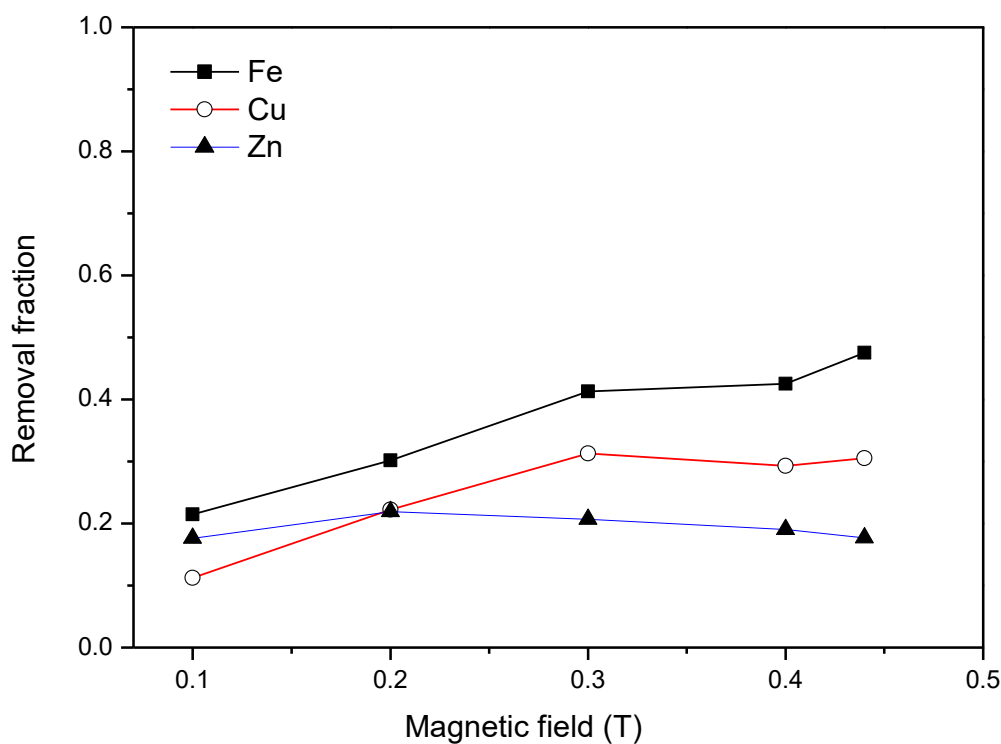


**Figure 3.** Metal removal fractions after magnetic separation under different magnetic fields.

In accordance with the properties of ferromagnetic materials, the magnetic susceptibility of Fe is at least  $10^6 \text{ m}^3/\text{kg}$  [31]. The magnetic force is therefore expressed with  $d_p$  in SI units as the follows:

$$F_M = (6.40 \times 10^{13}) \cdot d_p^3 \tag{11}$$

On the basis of the order of magnitude,  $F_g$  and  $F_B$  can be negligible because the particle size is smaller than  $10 \text{ }\mu\text{m}$ . Therefore, when  $F_M$  acting on the particles is stronger than  $F_D$ , the particles in the

fluid can be attracted to the magnetic filter and then separate from the waste sample after magnetic separation. For a ferromagnetic fragment, a particle size larger than 11 nm can result in  $F_M > F_D$ . By contrast, Cu and Zn removal did not apparently increase with the applied magnetic field because of their nonferromagnetic characteristics. However, during magnetic separation, parts of Cu and Zn were still removed with Fe from the waste. This phenomenon is because the fragment generated from sawing wire contained not only Cu and Zn but also Fe. Eventually, the removal fractions of Zn and Cu were lower than that of Fe. Increasing the cycle number of magnetic separation should enhance Fe removal from the waste. Figure 4 illustrates the effect of increasing cycle number on metal removal at 0.44 T. When the cycle number increased from 1 to 3, the Fe removal fraction increased linearly from 0.48 to 0.73. Because parts of Fe fragments contain Cu and Zn, Cu and Zn removal can be slightly enhanced by increasing the trap of Fe fragments in the magnetic filter. When the cycle number exceeded 3, the Fe removal fraction was saturated. Although the cycle number increased to 5, the Fe removal fraction increased to only 0.79.

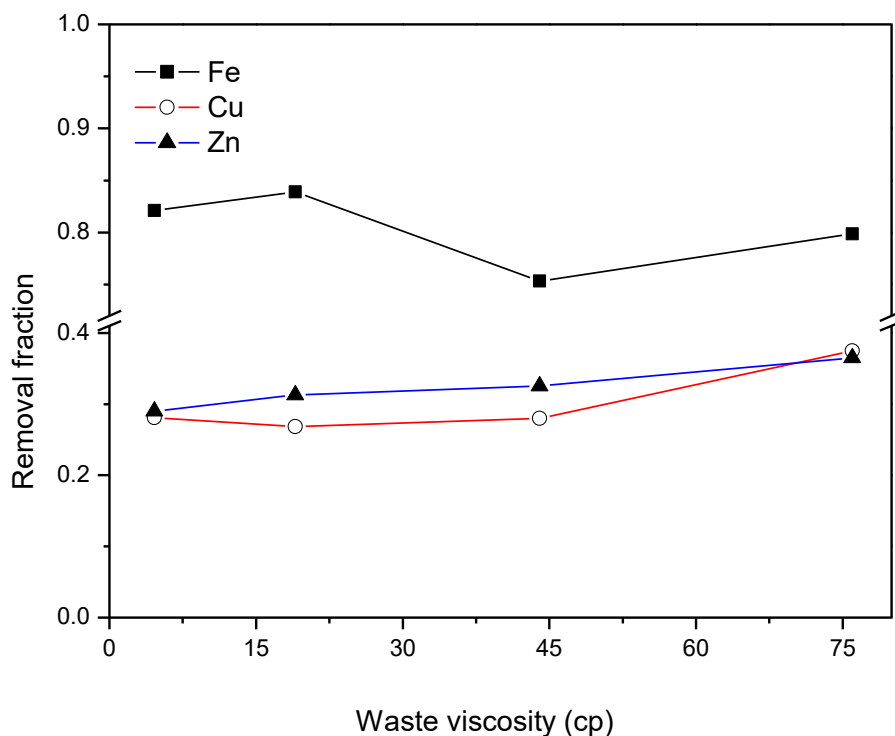


**Figure 4.** Effect of the passing number through the magnetic separator on metal removal fractions at 0.44 T.

The drag force  $F_D$  could be decreased by reducing the viscosity of the waste. A straightforward method for reducing its viscosity is by adding water. Magnetic separation performance can be expected to improve by decreasing  $F_D$ . Figure 5 shows the effect of waste viscosity adjusted using water on metal removal after the fifth cycle of magnetic separation at 0.44 T. The experimental results indicated that the removal fractions of Cu and Zn were not affected by viscosity. However, that of Fe could be

enhanced to more than 0.8. For example, when the viscosity of the waste was adjusted to 4.6 mPa·s, the removal fraction of Fe reached 0.82.

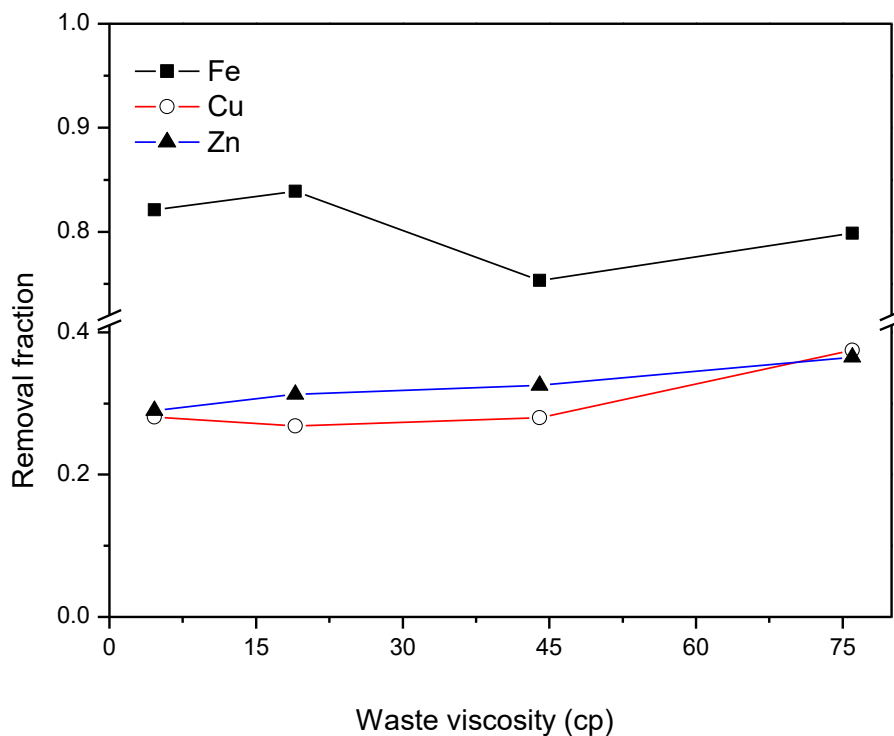


**Figure 5.** Effect of waste viscosity adjusted using water on metal removal fractions after the fifth magnetic separation at 0.44 T.

After magnetic separation, the PSD of the waste was altered, as shown in Fig. 6 (a). The size peak at 6.6  $\mu\text{m}$  decreased, but a peak appeared at 35  $\mu\text{m}$ . The particles of approximately 35  $\mu\text{m}$  in diameter may be attributed to Si or SiC fragments aggregating under the applied magnetic field because ultrasonic treatment (at 225 W for 30 min) could split the aggregated particles. The PSD of the waste after the ultrasonic treatment is shown in Fig. 6 (b), and no peak was detected at 35  $\mu\text{m}$ . This aggregation can be attributed to the magnetization of Fe under the magnetic field, causing attraction between particles, but the aggregated particles can be split through ultrasonic treatment.

After the magnetically treated waste was dried, the solid components of the waste were collected and analyzed using SEM and EDS. The analytical results are shown in Fig. 7. The SEM image reveals that several small particles adhered to one large particle; the EDS results at points A, B, and C indicate that the large particles (denoted by A and B) were mainly SiC, whereas the small particle (C) was Si. In addition, Fe was commonly observed on both particles A and B, indicating that the strength of adhesion between Fe and SiC was stronger than that between Fe and Si.

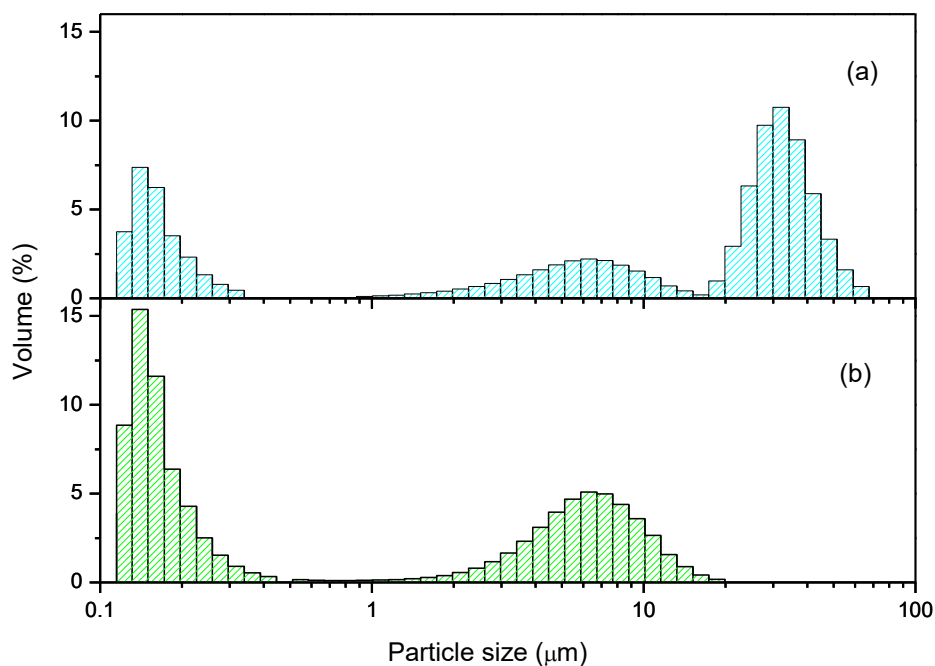


**Figure 6.** Particle size distribution of the collected sample (a) after magnetic separation; (b) after magnetic separation and subsequent ultrasonic treatment.

Nishijima et al. also reported that Fe tends to adhere to SiC, consistent with our observation [18]. Under a magnetic field, several small particles containing Fe aggregate into a large particle because of the magnetization of Fe. A large particle size, however, increases the drag force  $F_D$ . The SEM image also reveals that individual Fe fragments were seldom found in the waste. Therefore, a slight increase in Fe removal performance for diluted waste, shown in Fig. 5, can be attributed to the adhesion of Fe and aggregation of small particles. If aggregation is prevented, higher Fe removal performance is expected. Because the aggregated particles can be split through ultrasonic treatment after magnetic separation, a similar effect may be observed by performing ultrasonic treatment before magnetic separation. The separation results of ultrasonic pretreatment at 225 W for 30 min are shown in Fig. 8. When the waste was diluted with water to decrease its viscosity to 19 mPa·s and was pretreated through ultrasonic vibration, the removal of Fe through magnetic separation at 0.44 T was clearly enhanced. In particular, after five cycles of magnetic separation, the Fe removal fraction increased to 0.98, which is much higher than those without ultrasonic pretreatment. The ultrasonic pretreatment process efficiently enabled particle dispersion, resulting in  $F_M$  that was higher than  $F_D$  on more particles. However, Cu and Zn are nonferromagnetic, and their removal may be independent of the ultrasonic pretreatment.

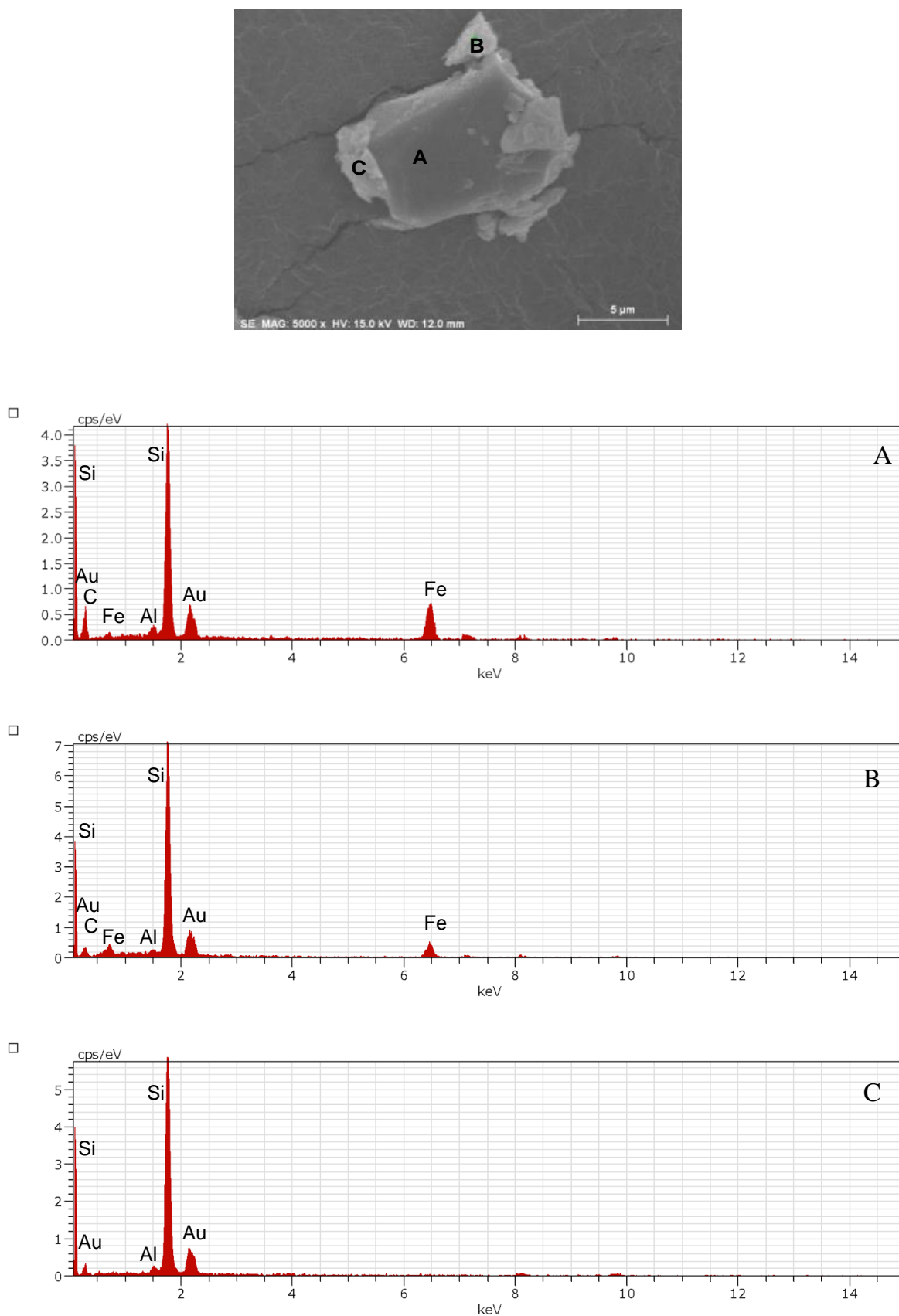
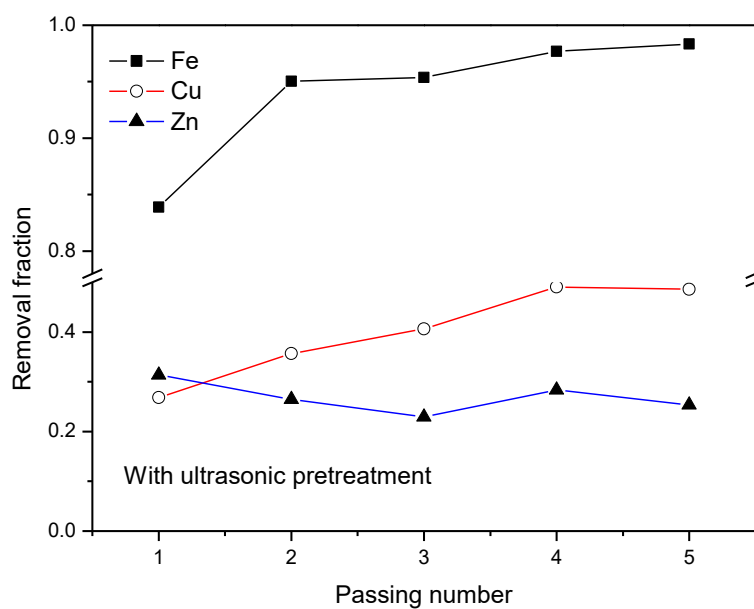
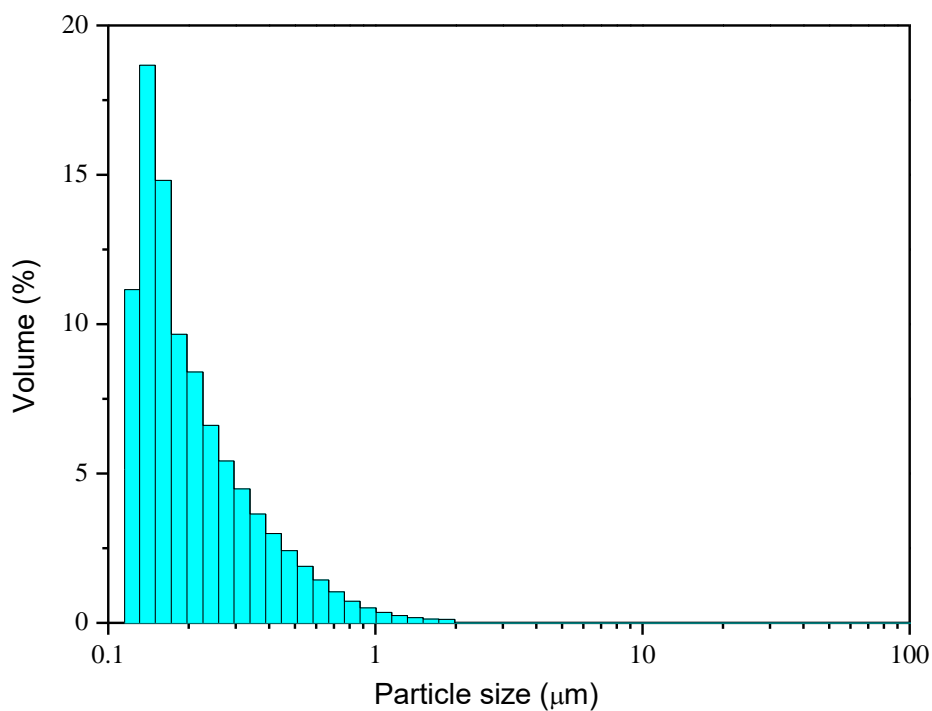


Figure 7. SEM images and EDS analysis of the obtained waste after removing liquids.



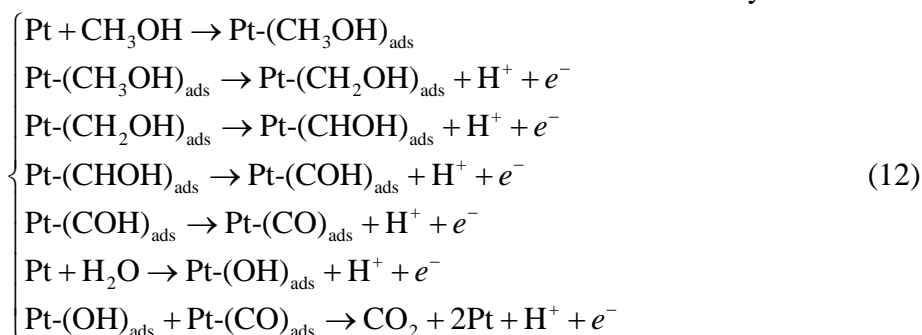
**Figure 8.** Effect of the passing number through the magnetic separator on metal removal fractions from the water-diluted waste (19 mPa·s) at 0.44 T with ultrasonic pretreatment.



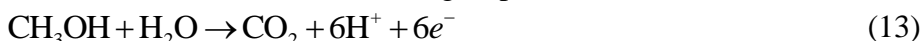
**Figure 9.** Particle size distribution of the recovered Si-rich powder.

The sample was collected at the outlet of the magnetic separator and was subsequently transferred to a centrifuge tube for size classification. The centrifugation process was conducted at 5000 rpm. For a Si particle of 1  $\mu\text{m}$  in diameter, traveling from the top of the centrifuge tube to the bottom takes approximately 11.95 min if the solid content is known at 112.1 g/L. Under the same conditions, a SiC particle of 1  $\mu\text{m}$  in diameter needs 7.36 min to travel from the top to bottom. Therefore, the centrifugation in this study was performed for 10 min at 5000 rpm to separate particles smaller than 1  $\mu\text{m}$ . Figure 9 shows the PSD of the upper-layer solution after centrifugation, indicating that only submicron-sized particles were observed. After filtrating and drying the upper-layer solution, analysis of the obtained powder showed that the contents of Si and Fe were 85 wt.% and 346 ppm, respectively. The powder collected from the upper-layer solution was denoted as res-Si (recycled-Si). The experimental results indicated that the Si content in the res-Si was twice that in the initial waste, and the total metal removal fraction reached 88.6%.

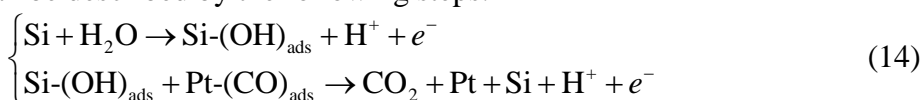
The res-Si was mixed with carbon Vulcan XC-72 (C) to prepare the catalyst support. Subsequently, Pt catalyst was deposited on this support for subsequent methanol electrooxidation. Figure 10 illustrates the linear sweep voltammograms of methanol electrooxidation when the Pt/C, Pt/C/Si, and Pt/C/res-Si catalysts were used. The voltammogram indicated a main current peak between 0.65 V and 0.70 V, similar to the findings of previous studies [25, 32–35]. The peak potentials for the three types of catalysts were close to each other, indicating that this peak corresponded to the same step of methanol oxidation catalyzed by Pt. Alternatively, Si particles would not change the reaction mechanism. During electrooxidation, the dehydrogenation of methanol occurs on Pt, and intermediates with carbonyl groups are subsequently formed with the release of electrons. The active sites on Pt are occupied by these intermediates. According to relevant studies [34], the possible reaction mechanism of the methanol oxidation can be described by the following steps:



In addition to the adsorption of methanol and its dehydrogenated products, the oxidation of water to form an adsorbed OH group is also a crucial factor. The active sites on Pt are released by the combination of the adsorbed OH and CO groups. The overall reaction can be described as



However, the current density of methanol electrooxidation catalyzed by Pt/C with Si was higher than that of catalysts without Si. This finding indicated that Si can enhance the release of active sites on Pt for further oxidation [26]. A possible reaction mechanism of the methanol oxidation with involvement of Si can be described by the following steps:



The effect of Si particles on Pt is similar to that of Ru on Pt. Pt mainly influences the dehydrogenation of methanol, whereas Si tends to provide an adsorbed OH group [32, 36–38]. They may together form  $\text{CO}_2$  and may release active sites for further oxidation.

Furthermore, the current density for the Pt/C/res-Si catalyst was approximately twice as high as that for the Pt/C catalyst at a scan rate of 50 mV/s. The Pt/C/Si catalyst contained commercial pure Si powder of 254 nm in diameter, whereas the largest possible particle size of the res-Si powder was 150 nm (shown in Fig. 9). Submicron-sized Si can enhance electrocatalysis, and fine Si particles can behave effectively. These results can be attributed to the fact that the fine Si-rich particles provide effective electrical contact between carbon supports and increase the specific surface area of the supports. In a previous study [26], fine catalytical particles were prepared using the sol-gel method and chemical etching, whereas the fine particles used in this study were collected from sawing waste. Our study presented a low-cost method for preparing catalyst and described a feasible method for waste reduction.

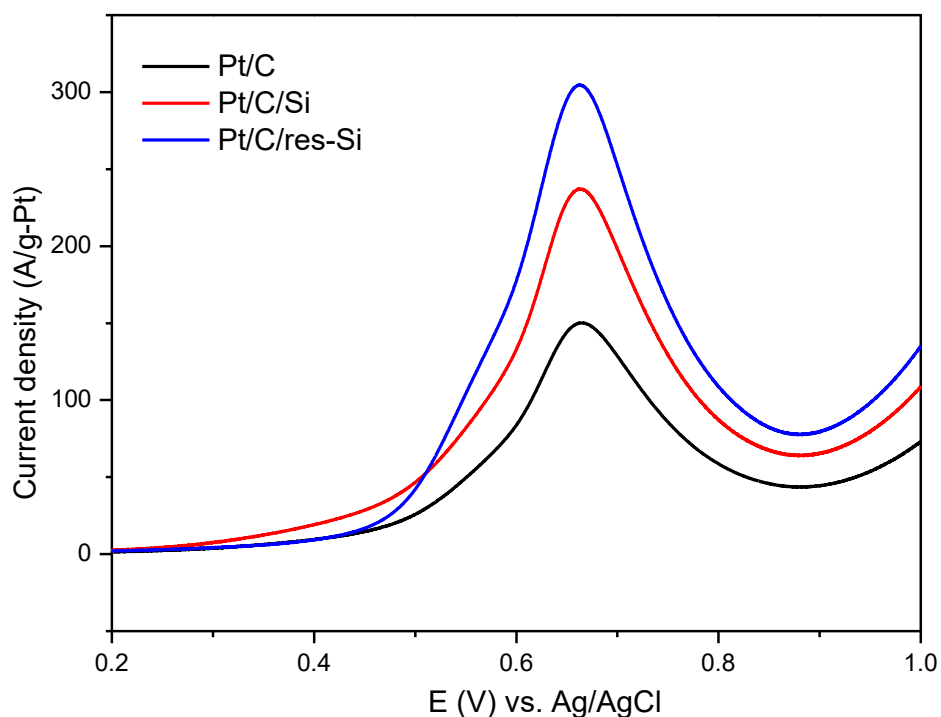


**Figure 10.** Linear sweep voltammograms of methanol electrooxidation by Pt/C, Pt/C/Si, and Pt/C/res-Si catalysts at a scan rate of 50 mV/s.

The electrode process can be observed through potential sweep at various rates. Figure 11 shows the dependence of the peak current on the square root of the scan rate. The results indicated that for the three types of catalysts, linear relationships were adequately maintained from 10 to 100 mV/s. This can be ascribed to a diffusion-controlled process mainly involving methanol [39, 40]. The slope of methanol electrooxidation catalyzed by Pt/C with Si was larger than that of catalysts without Si,

indicating once more that the catalysts with Si particles can provide a larger active surface area than those without Si.

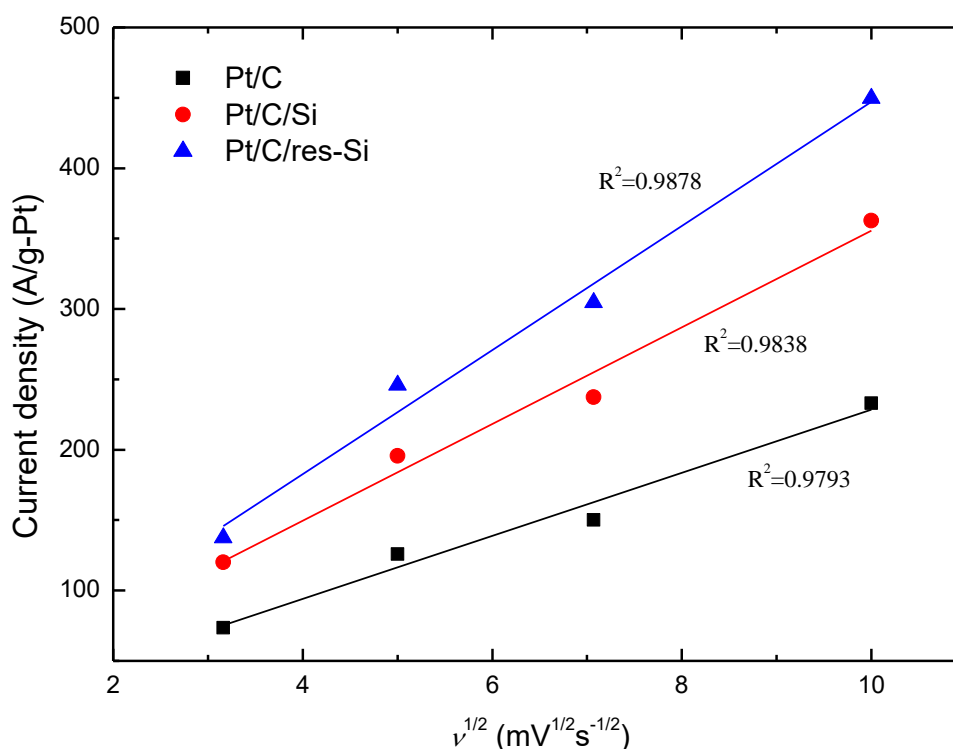


**Figure 11.** Dependence of the peak current on the square root of scan rate for Pt/C, Pt/C/Si and Pt/C/res-Si catalysts.

Through the procedures for recycling Si from the sawing waste suggested in this study, fine Si particles can be readily produced. Although the recycled Si-rich materials may not meet the requirements of wafer production for integrated chips or solar cells because of the Fe content, the fine Si-rich powder demonstrates high potential for electrocatalytic applications in energy devices, still representing the value of recycling.

#### 4. CONCLUSION

This paper proposes a process for recovering submicron-sized Si-rich powder with a low Fe content from Si sawing waste. The proposed process was performed at room temperature and involved ultrasonic treatment for particle dispersion, magnetic separation for Fe removal, and centrifugation for size classification. In magnetic separation, the effects of several operational variables on metal removal were studied, namely the applied magnetic field, waste viscosity, and the cycle number of flow through the magnetic separator. We observed that using ultrasonic treatment to perform particle

dispersion before magnetic separation is crucial for removing Fe. After centrifugation, the Si and Fe content in the recycled Si-rich powder were 85 wt.% and 346 ppm, respectively, and the powder size was in the submicron-order range. The res-Si was further mixed with carbon Vulcan XC-72 (C) prior to deposition of Pt to prepare the catalyst for methanol electrooxidation. The linear sweep voltammetry results indicated that the current density of methanol electrooxidation for the Pt/C/res-Si catalyst was higher than that for the Pt/C catalyst and that for the Pt/C/Si catalyst. Thus, we conclude that the submicron-sized recycled Si powder can be purified further to form a wafer for solar cells or can be applied directly to enhance the electrocatalyst for energy devices.

#### ACKNOWLEDGMENTS

The authors would like to thank the National Science Council of Taiwan for financially supporting this research (Contract No. NSC 101-2221-E-027-109-MY3) and Sino-American Silicon Products, Inc., for its material assistance. This manuscript was edited by Wallace Academic Editing.

#### References

1. D. Sarti, R. Einhaus, *Solar Energy Materials and Solar Cells*, 72 (2002) 27.
2. T. Neesse, *interceram*, 55 (2006), 430.
3. N. Drouiche, P. Cuellar, F. Kerkar, S. Medjahed, N. Boutouchent-Guerfi, M. O. Hamou, *Renewable & Sustainable Energy Reviews*, 32 (2014) 936.
4. A. Ciftja, L. Zhang, A. Kvithyld, T. A. Engh, *Rare Metals*, 25 (2006) 180.
5. L. Zhang, A. Ciftja, *Solar Energy Materials and Solar Cells*, 92 (2008) 1450.
6. T. Y. Wang, Y. C. Lin, C. Y. Tai, R. Sivakumar, D. K. Rai, C. W. Lan, *Journal of Crystal Growth*, 310 (2008) 3403.
7. T. Y. Wang, Y. C. Lin, C.Y. Tai, C. C. Fei, M. Y. Tseng, C. W. Lan, *Progress in Photovoltaics: Research and Applications*, 17 (2009) 155.
8. D. Li, P. Xing, Y. Zhuang, F. Li, G. Tu, *Transactions of Nonferrous Metals Society of China*, 24 (2014) 1237.
9. Y. C. Lin, T. Y. Wang, C. W. Lan, C. Y. Tai, *Powder Technology*, 200 (2010) 216.
10. Y. Xiao, Y. Yang, *Advanced Materials Research*, 295-297 (2011) 2235.
11. M. Huang, Y. Xiong, X. Wei, C. Yin, L. Zhou, *Electronic Components & Materials*, 29 (2010) 74.
12. Y. C. Lin, C. Y. Tai, *Separation and Purification Technology*, 74 (2010) 170.
13. H. P. Hsu, W. P. Huang, C. F. Yang, C. W. Lan, *Separation and Purification Technology*, 133 (2014) 1.
14. H. Y. Wang, Y. Tan, J. Y. Li, Y. Q. Li, W. Dong, *Separation and Purification Technology*, 89 (2012) 91.
15. J. Li, K. Huang and H. Zhu, *Chemical Engineering Science*, 127 (2015) 25.
16. K. Tomono, H. Furuya, S. Miyamoto, Y. Okamura, M. Sumimoto, Y. Sakata, R. Komatsu, M. Nakayama, *Separation and Purification Technology*, 103 (2013) 109.
17. S. Liu, K. Huang, H. Zhu, *Separation and Purification Technology*, 118 (2013) 448.
18. S. Nishijima, Y. Izumi, S. I. Takeda, H. Suemoto, A. Nakahira, S. I. Horie, *IEEE Transactions on Applied Superconductivity*, 13 (2003) 1596.
19. A. V. Hariharan and J. Ravi, *Recovery of Silicon from Kerf Silicon Waste*, U.S. Patent 0032630 A1 (2010).
20. P. Hoffmann, *Method for recovering silicon from sawing waste*, W.O. Patent 081245 (2009).
21. T. H. Tsai, J. H. Huang, *Journal of the Taiwan Institute of Chemical Engineers*, 40 (2009) 1.

22. T. H. Tsai, *Separation and Purification Technology*, 68 (2009) 24.
23. T. H. Tsai, *Separation and Purification Technology*, 46 (2011) 702.
24. W. Shimizu, K. Okada, Y. Fujita, S. Zhao, Y. Murakami, *Journal of Power Sources*, 205 (2012) 24.
25. K. Nam, S. Lim, S. K. Kim, S. H. Yoon, D. H. Jung, *International Journal of Hydrogen Energy*, 37 (2012) 4619.
26. B. Liu, J. H. Chen, X. X. Zhong, K. Z. Cui, H. H. Zhou, Y. F. Kuang, *Journal of Colloid and Interface Science*, 307 (2007) 139.
27. N. Pamme, *Lab Chip*, 6 (2006) 24.
28. S. S. Shevkoplyas, A. C. Siegel, R. M. Westervelt, M. G. Prentiss, G. M. Whitesides, *Lab Chip*, 2007, 7 (2007) 1294.
29. W. Leung, *Industrial Centrifugation Technology*, McGraw-Hill, New York (1998).
30. J. F. Richardson, W. N. Zaki, *Chemical Engineering Science*, 3 (1954) 65.
31. D. W. Callister and D. G. Rethwisch, *Materials Science and Engineering: An Introduction*, 7th ed., John Wiley & Sons, Inc. New York (2007).
32. A. B. Kashyout, Abu Bakr A.A. Nassr, L. Giorgi, T. Maiyalagan, Bayumy A. B. Youssef, *International Journal of Electrochemical Science*, 6 (2011) 379.
33. Y. Ma, R. Wang, H. Wang, S. Ji, *International Journal of Electrochemical Science*, 8 (2013) 6085.
34. Q. Dong, Y. Li, L. Zhu, T. Ma, C. Guo, *International Journal of Electrochemical Science*, 8 (2013) 8191.
35. M. C. L. dos Santos, R. M. Dutra, V. A. Ribeiro, E. V. Spinacé, A. O. Neto, *International Journal of Electrochemical Science*, 12 (2017) 3549.
36. A. Galal, N. F. Atta, H. K. Hassan, *International Journal of Electrochemical Science*, 7 (2012) 768.
37. C. W. Kuo, Z. Y. Kuo, J. J. Jow, T. Y. Wu, J. Y. Chen, X. X. Zhu, *International Journal of Electrochemical Science*, 7 (2012) 4974.
38. C. Li, R. Dai, R. Qi, X. Wu and J. Ma, *International Journal of Electrochemical Science*, 12 (2017) 2485.
39. K. Honda, M. Yoshimura, T. N. Rao, D. A. Tryk, A. Fujishima, K. Yasui, Y. Sakamoto, K. Nishio, H. Masuda, *Journal of Electroanalytical Chemistry*, 514 (2001) 35.
40. A. J. Bard and L. R. Faulkner, *Electrochemical Methods*, 2nd ed., John Wiley and Sons, New York (2001).